Computational and Structural Biotechnology Journal 21 (2023) 3564–3574

Contents lists available at ScienceDirect

Computational and Structural Biotechnology Journal

journal homepage: www.elsevier.com/locate/csbj

Research article

Autophagy and biotransformation affect sorafenib resistance in hepatocellular carcinoma

Ruiqi Zheng [a,1], Shuang Weng [b,1], Jianping Xu [c,1], Zhuo Li [d], Yaru Wang [a], Zulihumaer Aizimuaji [a], Sheng Ma [a], Linlin Zheng [e], Haiyang Li [e], Wantao Ying [b,f,*], Weiqi Rong [e,*], Ting Xiao [a,**]

[a] State Key Laboratory of Molecular Oncology, Department of Etiology and Carcinogenesis, Beijing Key Laboratory for Carcinogenesis and Cancer Prevention, National Cancer Center/National Clinical Research Center for Cancer/Cancer Hospital, Chinese Academy of Medical Sciences and Peking Union Medical College, Beijing 100021, China
[b] State Key Laboratory of Proteomics, National Center for Protein Sciences (Beijing), Beijing Proteome Research Center, Beijing Institute of Lifeomics, Beijing 102206, China
[c] Department of Medical Oncology, National Cancer Center/National Clinical Research Center for Cancer/Cancer Hospital, Chinese Academy of Medical Sciences and Peking Union Medical College, No. 17 Panjiayuan Nanli, Beijing 100021, China
[d] Department of Pathology, National Cancer Center/National Clinical Research Center for Cancer/Cancer Hospital, Chinese Academy of Medical Sciences and Peking Union Medical College, No. 17 Panjiayuan Nanli, Beijing 100021, China
[e] Department of Hepatobiliary Surgery, National Cancer Center/National Clinical Research Center for Cancer/Cancer Hospital, Chinese Academy of Medical Sciences and Peking Union Medical College, Beijing 100021, China
[f] College of Life Science and Bioengineering, Beijing University of Technology, No. 100, Pingleyuan, Chaoyang District, Beijing 100124, China

ARTICLE INFO

Article history:
Received 17 April 2023
Received in revised form 22 June 2023
Accepted 4 July 2023
Available online 5 July 2023

Keywords:
Sorafenib resistance
Autophagy
Biotransformation
Proteomics
HCC
PI3K/AKT/mTOR

ABSTRACT

As sorafenib is a first-line drug for treating advanced hepatocellular carcinoma, sorafenib resistance has historically attracted attention. However, most of this attention has been focused on a series of mechanisms related to drug resistance arising after sorafenib treatment. In this study, we used proteomic techniques to explore the potential mechanisms by which pretreatment factors affect sorafenib resistance. The degree of redundant pathway PI3K/AKT activation, biotransformation capacity, and autophagy level in hepatocellular carcinoma patients prior to sorafenib treatment might affect their sensitivity to sorafenib, in which ADH1A and STING1 are key molecules. These three factors could interact mechanistically to promote tumor cell survival, might be malignant features of tumor cells, and are associated with hepatocellular carcinoma prognosis. Our study suggests possible avenues of therapeutic intervention for patients with sorafenib-resistance and the potential application of immunotherapy with the aim of improving the survival of such patients.

Abbreviations: **HCC**, Hepatocellular carcinoma; **ACLY**, Adenosine triphosphate citrate lyase; **SIRT6**, Sirtuins 6; **EGFR**, Epidermal growth factor receptor; **HGF**, Hepatocyte growth factor; **IGF**, Insulin like growth factor; **STING1**, Stimulator of interferon response cGAMP interactor 1; **ADH1A**, Alcohol dehydrogenase 1 A; **MTOR**, Mechanistic target of rapamycin kinase; **HLA-DR**, Human leukocyte antigen-DR; **CGAS**, Cyclic GMP-AMP synthase; **HDAC1**, Histone deacetylase 1; **ADCD**, Autophagy-dependent cell death; **NLRP3**, NOD-like receptor thermal protein domain associated protein 3; **TAMs**, Tumor-associated macrophages; **APCs**, Antigen-presenting cells

* Corresponding author at: State Key Laboratory of Proteomics, National Center for Protein Sciences (Beijing), Beijing Proteome Research Center, Beijing Institute of Lifeomics, Beijing 102206, China.
** Corresponding authors.
E-mail addresses: yingwantao@ncpsb.org.cn (W. Ying), dr_rongweiqi@163.com (W. Rong), xiaot@cicams.ac.cn (T. Xiao).
[1] Equal contributors.

https://doi.org/10.1016/j.csbj.2023.07.005

1. Introduction

According to Global Cancer Statistics 2020, primary liver cancer is the sixth most common cancer and the third leading cause of cancer death worldwide, with a particularly high incidence in East Asia, where 75–85% of the pathological types are Hepatocellular carcinoma (HCC) [1]. HCC has an insidious onset and low rate of early diagnosis and is usually seen in patients with chronic hepatitis associated with viral infections, alcohol abuse, or metabolic syndrome. Advanced HCC is not sensitive to radiotherapy or chemotherapy [2,3]. Sorafenib, a first-line drug for treating advanced HCC, is an oral multikinase inhibitor. It targets RAF, c-Kit, Flt-3, and RET in tumor cells as well as the vascular endothelial growth factor receptor (VEGFR) and platelet-derived growth factor receptor (PDGFR) in vascular endothelial cells [4–6]. However, pathways such as the epidermal growth factor receptor (EGFR), PI3K/AKT/mTOR, hepatocyte growth factor (HGF)/c-Met, and insulin-like growth factor (IGF)/IGFR pathways are associated with the development of HCC [7].

Due to the more limited target of sorafenib, only approximately 30% of patients benefit from sorafenib, and individuals in these populations usually acquire resistance within 6 months of treatment initiation [3]. The mechanisms associated with resistance following sorafenib administration have received sufficient attention. Sorafenib treatment is currently thought to activate resistance mechanisms such as those mediated by noncoding RNAs, upregulation of proangiogenic signaling pathways, activation of the PI3K/AKT/mTOR pathway, abnormal intracellular pharmacokinetics and the hypoxic tumor microenvironment [5,8]. However, considering the low patient benefit rate of sorafenib, there is also clinical value in predicting patients' sensitivity to sorafenib through evaluation of pretreatment factors to adjust treatment regimens. In addition, sorafenib resistance is considered to be reversible [5]: in a mouse model study, sorafenib-resistant HCC tumor cells from one mice were isolated and transplanted into another mice, and the transplanted tumors were not found to be resistant to sorafenib in the new host, i.e., the sorafenib-resistant phenotype is not propagated [9]; another study found that inhibition of adenosine triphosphate citrate lyase (ACLY), a key enzyme in lipid metabolism, reversed the resistance phenotype in sorafenib-resistant hepatocellular carcinoma cell lines HepG2 and Huh7 [10]; in renal cell carcinoma, Ubenimex was found to inhibit Akt expression and enhance autophagy, promote apoptosis in 786-O-R cell line and reverse resistance to sorafenib, silencing of the apoptosis-inhibiting mucin MUC13 also had this effect [11,12]; in gastric cancer studies, sorafenib resistance in cell lines was overcome by silencing Sirtuins 6 (SIRT6) to promote ferroptosis [13]. Alterations in the sorafenib resistance phenotype have been observed in many of the above tumor types in many aspects of modulation, and we therefore believe that modulating the relevant influences prior to treatment may improve patient outcomes.

Among the pretreatment factors, autophagy helps cells maintain homeostasis by recycling aged or damaged organelles and is an essential means for cells to cope with survival stress in a harsh environment [14]. Biotransformation is a vital function of the liver, and although biotransformation is not equivalent to detoxification, it can reduce the toxicity of most substrates and render them readily excreted. The phase II reactions in biotransformation include glucuronidation, sulfation, methylation, acetylation, glutathione binding, and amino acid binding [15]. Autophagy and biotransformation may profoundly affect patient sensitivity to sorafenib. In this study, we performed proteomic analysis of the tissues of 16 Chinese HCC patients after postoperative relapse prior to sorafenib treatment and partially explained how some of the pretreatment factors, represented by autophagy and biotransformation, interact and thus influence the efficacy of subsequent sorafenib treatment.

2. Materials and methods

2.1. Sample collection

We obtained surgical resection samples from 16 HCC patients before sorafenib treatment for proteomic analysis. These patients were started on sorafenib because of recurrence after radical hepatectomy. According to the American Joint Committee on Cancer (AJCC) 8th, the starting dose of sorafenib is 400 mg bid, and the dosage is adjusted during the course of treatment according to the patient's side effects, until the course of treatment is stopped when the patient becomes resistant to sorafenib. Seven patients (X1–7) were deemed to respond to sorafenib treatment, and the remaining nine were deemed nonresponding (X8–16) by more than two clinical internists. The criteria for response classification were as follows: patients with disease progression within 6 months of sorafenib administration were classified as nonresponders, while those without disease progression and those with tumor shrinkage were classified as responders. All biological specimens were obtained from the Cancer Institute/Hospital, Peking Union Medical College, with the approval of the Research Ethics Committee. None of the patients received any preoperative targeted therapy. The resected specimens were fixed with formalin and preserved by paraffin embedding. Histological diagnosis of HCC was performed by pathologists. Hematoxylin and eosin (HE)-stained slides were used to assess tumor purity, and 16 HCC tissues with tumor purity > 50% were selected for proteomic profiling. The clinical information is shown in Table S1.

2.2. Processing of LC-MS/MS

2.2.1. Protein extraction

Samples were sequentially soaked in fresh xylene, absolute ethanol, 85% ethanol, 70% ethanol, and 50% ethanol with shaking at a constant speed. Tissues were removed from the dried glass slides by scraping with 1 ml of precooled PBS, left at room temperature for 5 min, and then centrifuged at 14000g for 15 min to separate and remove the supernatant. Then, 150 µl of freshly prepared lysis buffer (1% sodium dodecyl sulfate and 2 mM dithiothreitol (DTT) in 0.1 M Tris-HCl; 10 µl protease inhibitor per 1 ml (Roche, REF 04693116001)) was added to the pellet and incubated at 99 °C for 30 min. The lysate was naturally cooled to room temperature, and subjected to 99 cycles of sonication (power 180 W, 1- s on and 2- s off). The lysate was again incubated at 99 °C for 30 min and naturally cooled to room temperature. Then, the lysate was centrifuged at 14000g for 15 min, and the supernatant was collected and stored at −80 °C before use.

2.2.2. Protein digestion

Proteins were digested by filter-assisted sample preparation (FASP) [16,17]. In brief, each sample was diluted to 1.5 ml with UA solution (8 M urea in 0.1 M Tris-HCl), and the supernatant was sequentially added to a 30 kD filter for centrifugation. Next, 200 µl of UA solution was added, and the sample was washed once by centrifugation. Then, 100 µl of DTT solution (20 mM DTT in UA solution) was added, and the sample was incubated at 37 °C for 4 h. After the DTT solution was removed by centrifugation, 100 µl of IAA solution (50 mM iodoacetamide dissolved in UA solution) was added, and the reaction was allowed to proceed at room temperature for 30 min in the dark. The ultrafractionation tube was washed twice with 200 µl of UA and three times with 200 µl of ABC solution (50 mM ammonium bicarbonate in water, pH 8.5) by centrifugation. Next, 100 µl of ABC solution containing 1 µg of trypsin was added to each filter tube, and the tubes were sealed and incubated at 37 °C for 16 h. Peptides were collected by centrifugation at 14000g and dried at 45 °C. The

peptide mixture was resolved with buffer A (0.1% formic acid) and quantified using a Nano-drop OneC spectrophotometer.

2.2.3. Liquid chromatography tandem mass spectrometry analysis

The liquid chromatography-tandem mass spectrometry (LC–MS/MS) detection system consisted of a nanoflow high-performance liquid chromatography (HPLC) instrument (Easy nLC1200, Thermo Fisher) coupled to an Orbitrap Q-Exactive HF mass spectrometer (Thermo Fisher). For acquisition of mass spectra, the optimal data-independent acquisition (DIA) parameters described in the article by Shuang Weng et al. [18] were used. In brief, 2 μg of the peptide mixture resolved with buffer A was loaded on a 30-cm self-packing column (150-μm inner diameter, ReproSil-Pur C18-AQ, 1.9 μm; Dr. Maisch) with a 120-min LC gradient time (Table S2) at a flow rate of 600 nl/min. The chromatograph peak width was 18 s. A standard amount of iRT spike-in was added to ensure calibration. The MS1 survey scan range was 400–1200 *m/z*, and the MS1 scan was followed by 32 MS2 scans with overlapping sequential precursor isolation windows (25 *m/z* isolation width, 1 *m/z* overlap). For the MS2 survey scan, the automatic gain control (AGC) target was set to 3e6, and the maximum injection time (IT) was set to 45 ms.

2.2.4. Protein identification by Spectronaut-based database searching

The raw data files obtained from the mass spectrometry analysis were imported into SpectronautTM software for processing, and the spectral library was selected from the human liver cancer proteome spectral library established in the article by Shuang Weng et al. [18]. The false discovery rate (FDR) threshold at the protein and peptide levels was set to 0.01. Peak areas at the MS2 level were selected for protein and peptide quantitation. Subsequent in-depth processing was performed using data packages in R software.

2.3. Proteomic data analysis

2.3.1. Sample quality control and data normalization

Boxplots were used to visualize the numbers of identified components at three levels: protein group, peptide, and precursor. No sample exhibited an extremely high or low number of identified components (Fig. S1), and all samples were included in subsequent analysis. Protein expression matrices were quantile normalized using the limma package (v 3.42.2) in R/Bioconductor. We further processed the expression matrix using the removeBatchEffect() function of limma (v 3.52.4), and subsequent analysis was limited to the 5209 genes expressed in at least 50% of the samples (Table S3). For algorithms that could not handle missing values, we used mice (v 3.15.0) [19] to fill in the missing values by a multiple interpolation method.

2.3.2. Bioinformatics analysis of proteome data

Analysis of differential protein expression between nonresponders and responders was performed using limma (v 3.52.4) [20], with the following criteria: $p \le 0.05$ and $|logFC| \ge 1$. We then used clusterProfiler (v 4.4.4) [21] to perform Kyoto Encyclopedia of Genes and Genomes (KEGG) pathway enrichment analysis and gene set enrichment analysis (GSEA) on the differentially expressed protein, GSVA (v 1.44.5) to perform single-sample gene set enrichment analysis (ssGSEA) [22], Xcell (v 1.1.0) for immune infiltration analysis [23], ConsensusClusterPlus (v 1.60.0) for consensus clustering [24], and surv (v 3.4–0) and survminer (v 0.4.9) for survival analysis. We also obtained data from related studies by Jia Fan et al. and Fuchu He et al. for further validation [17,25]. Statistical analyses were performed on R version 4.2.1. For analysis of paired group data, the Wilcoxon signed-rank test was used. Statistical significance was accepted at $p < 0.05$ or a Benjamini–Hochberg adjusted p value < 0.05.

2.4. Immunohistochemistry (IHC) and Scoring

Sections were baked at 65 °C for 4 h, deparaffinized with xylene and ethanol, and then incubated with 3% H_2O_2 for 10 min in the dark to quench endogenous peroxidase activity. After antigen retrieval by heating in citrate repair solution (pH= 6.0) or EDTA buffer (pH= 9.0) in a microwave oven for 10 min, the sections were blocked with goat nonimmune serum and incubated with primary antibodies against ADH1A (1:1000, Abcam), STING1 (1:10000, Proteintech), CD163 (1:400, Cell Signaling), CD8 (1:200, Cell Signaling) and HLA_DRB (1:2000, Abcam) overnight at 4 °C. After incubation with secondary antibodies, a chromogenic reaction was performed using the DAB kit. The sections were then counterstained with hematoxylin. Staining was analyzed and scored by two experienced pathologists. Samples were scored on a scale from 0 to 3 (0, negative; 1, weakly positive; 2, moderately positive; 3, strongly positive) based on the intensity of staining and the percentage of positive staining. The staining intensity score was multiplied by the percentage of the slices exhibiting staining for the object of interest to calculate the “Hscore” of the object of interest. The details of the reagents used are shown in Table S4.

3. Results

3.1. Global proteomic profiling of sorafenib-nonresponding and sorafenib-responding HCC patients

To study the characteristics of patients with HCC exhibiting different treatment effects of sorafenib, we performed proteomic mass spectrometry on formalin-fixed paraffin-embedded HCC tissue samples from 16 patients before sorafenib treatment (Fig. S2A). Among the patients, 7 responded to sorafenib treatment, and the other 9 who did not. By using Spectronaut software for database searching, only the proteins that were reliably quantified (Q value < 0.01) were output; a total of 7177 proteins were quantified, with an average of 5139 proteins quantified per sample (Fig. S2B). Across the samples, 3063 proteins were quantified in all samples. We examined the distribution of all protein abundances, and found that it was unimodal for all 16 samples (Fig. S2C). After data normalization, each sample was clustered with the same distribution (Fig. S2D).

3.2. Differential proteomic analysis of the sorafenib-nonresponding and sorafenib-responding groups of HCC patients

A standard spartial least squares regression analysis approach (PLS_DA) was used to classify samples from the sorafenib-related proteomic profile data and the drug-nonresponding and drug-responding groups were found to be distinguishable (Fig. 1A), with a significant difference in protein expression characteristics between the two groups. Differential analysis identified a total of 29 differentially expressed proteins, 14 of which were upregulated in the drug-nonresponding group and 15 in the responding group (Fig. 1D). Among these proteins, stimulator of interferon response cGAMP interactor 1 (STING1) (Fig. 1B, P = 0.0310), which was upregulated in the nonresponding group, and alcohol dehydrogenase 1A (ADH1A) (Fig. 1C, P = 0.1700), which was upregulated in the responding group were the core proteins selected for our exploration of pretreatment factors affecting sorafenib resistance. The STING1 protein is an essential regulator of autophagy [26,27], while the ADH1A protein is an important member of an enzyme family involved in biotransformation [25].

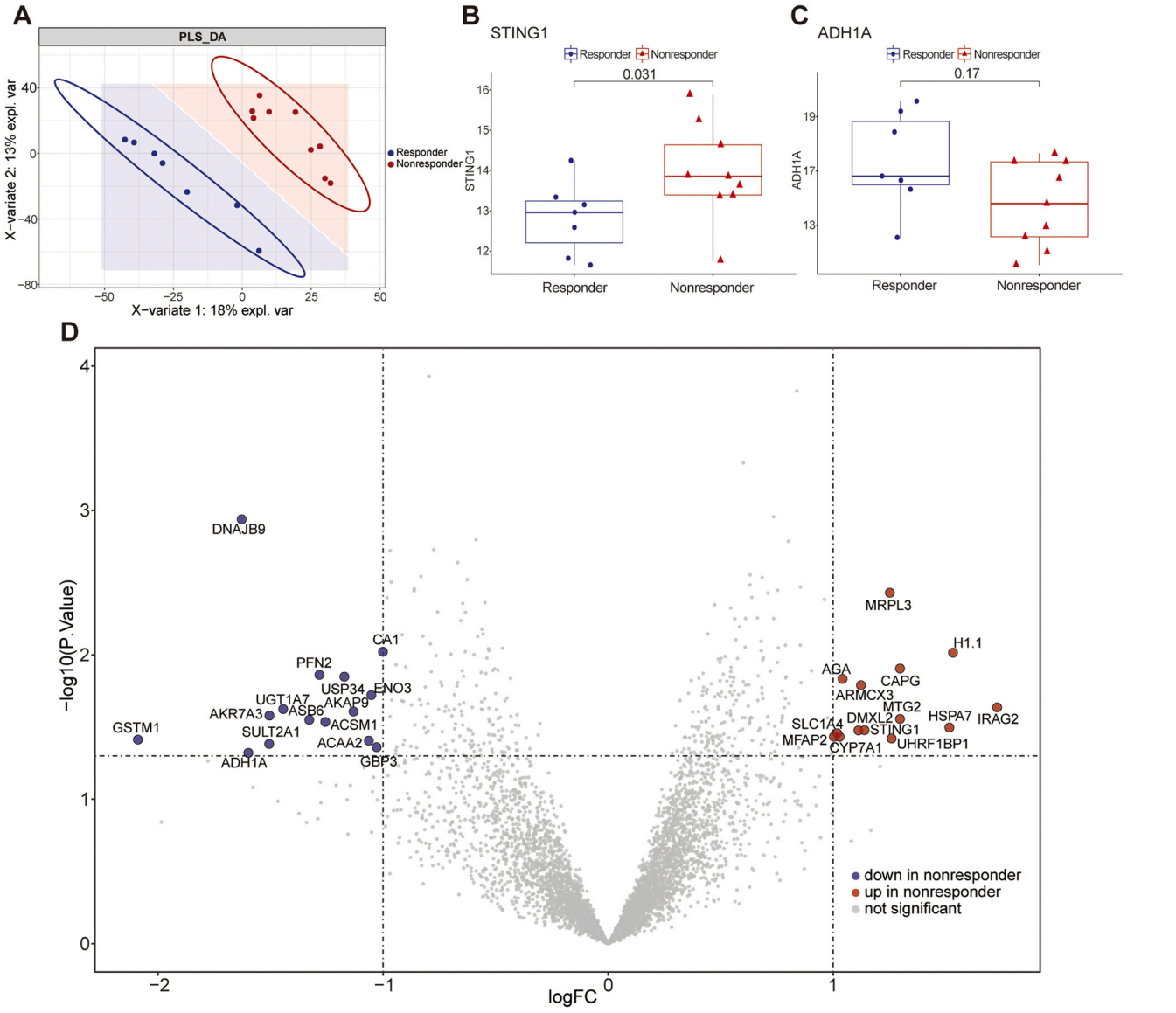

Fig. 1. Differential analysis of sorafenib protein profile data. (A) PLS-DA can distinguish between the drug-nonresponding and drug-responding groups. (B) and (C) Expression of STING1 and ADH1A, as measured by mass spectrometry, in the two groups. (D) Volcano plot showing the differentially expressed proteins identified.

3.3. Autophagy-related and biotransformation-related pathways differ between the responding and nonresponding groups

KEGG enrichment analysis of the screened identified expressed proteins revealed that the ascorbate and aldarate metabolism, retinol metabolism, pentose and glucuronate interconversions, and glutathione metabolism pathways which are associated with biotransformation [28] were enriched in the responding group, while the lysosome and cytosolic DNA sensing pathway, which are associated with autophagy, were enriched in the drug-nonresponding group (Fig. 2A, Table S5-6) [29]. The protein expression profile data were converted to single-sample pathway enrichment scores using ssGSEA, and the Wilcoxon signed-rank test was used to evaluate the significance of differences between the two groups. Annotation via c2.cp.kegg.v2022.1. Hs.symbols.gmt revealed that the glycolysis gluconeogenesis and nicotinate and nicotinamide metabolism pathways were enriched in the responding group. In contrast, the cytosolic DNA sensing, VEGF signaling, and mTOR signaling pathways were enriched in the nonresponding group, and there was no difference in MAPK signaling pathway enrichment between the two groups (Table S7). Further annotation by c2.cp.reactome.v2022.1. Hs.symbols.gmt and c2.cp.wikipathways.v2022.1. Hs.symbols.gmt revealed that the PI3K/AKT/mTOR pathway was significantly enriched in the nonresponding group (Fig. 2B, Table S8-9). It has been reported that mTOR inhibits the transcription of ADH1A by phosphorylating histone deacetylase 1 (HDAC1) [30], and our analysis in mass spectrometry data revealed a trend of upregulation of HDAC1 in the drug- nonresponding group (Fig. S4A, P = 0.3000). GSEA of the pentose and glucuronate interconversions pathway, representing biotransformation, and the lysosome pathway, representing autophagy, also demonstrated significant differences between the two groups in these two aspects (Fig. 2C).

3.4. Immune infiltration analysis suggests immune potential in the nonresponding group

Analysis of differences in the infiltration of each cell type in the drug-nonresponding and drug-responding groups using Xcell revealed that CD8 + T cells (Fig. 3A, P = 0.0638), natural killer T (NKT) cells (Fig. 3A, P = 0.0128), M2 macrophages (Fig. 3A, P = 0.0108), gamma delta T (Tgd) cells (Fig. 3A, P = 0.0258), B cells (Fig. 3A, P = 0.0164), endothelial cells (Fig. 3A, P = 0.0311) and pericytes

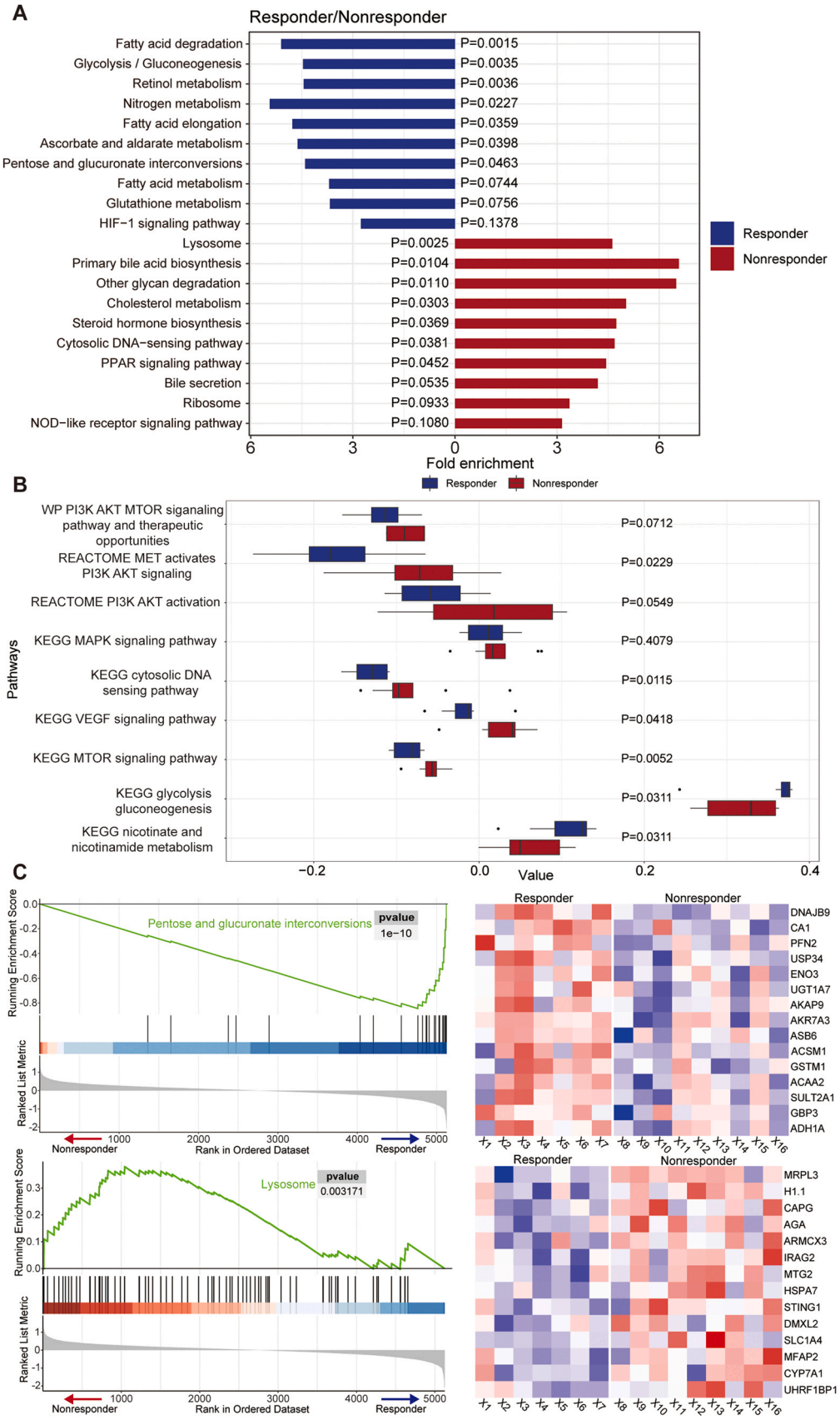

Fig. 2. Pathway enrichment analysis. (A) KEGG enrichment analysis revealed the upregulation of autophagy-related pathways in the nonresponding group and the upregulation of biotransformation-related pathways in the responding group. (**B**) ssGSEA was performed to convert expression profiles into pathway enrichment scores, and the Wilcoxon signed-rank test was performed to identify differential pathways between the two groups. (**C**) GSEA of representative pathways for biotransformation and autophagy. The heatmap on the right shows the differentially expressed proteins in the two groups.

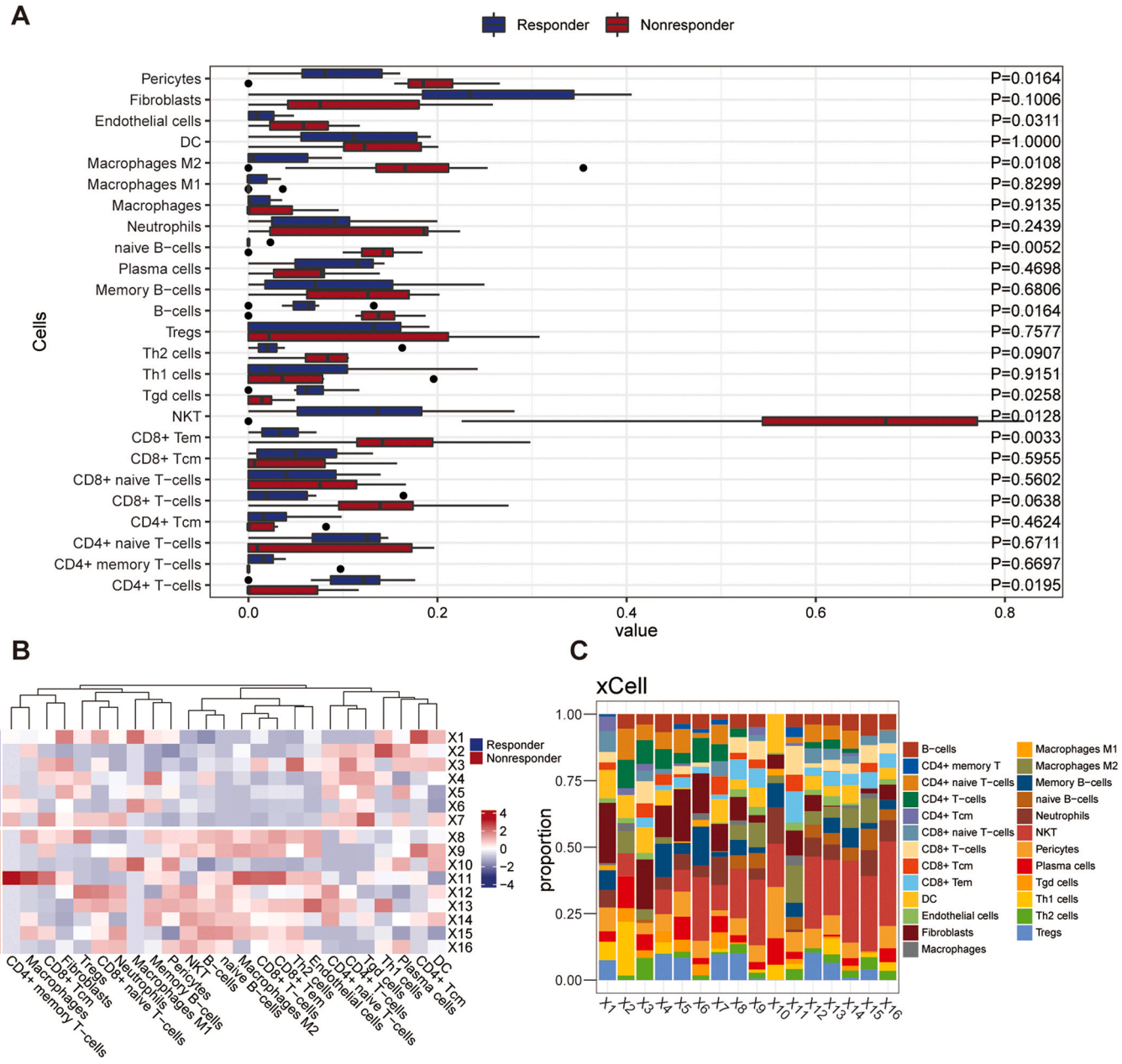

Fig. 3. Immune infiltration analysis. (A) Box plot showing the differences between the drug-nonresponding and drug-responding groups for each infiltrating cell type. (B) and (C) The heatmap and stacked plot show the abundance of each infiltrated cell type in each sample.

(Fig. 3A, P = 0.0164) were highly infiltrated in the nonresponders, and that CD4 + T cells (Fig. 3A, P = 0.0195) were highly infiltrated in the responders (Table S10). The same is true for the content and proportional structure of the above cells in the heatmap and stacking plot between the two groups (Fig. 3B-C). Innate immunocytes were exhibited significantly high infiltration in the nonresponding group. Interestingly, both immunosuppressive and immunoreactive cells were also highly infiltrated in the nonresponding group.

3.5. Immunohistochemical analysis shows a trend consistent with the immune infiltration analysis

The Hscore was defined as the staining intensity multiplied by the percentage of the section exhibiting staining for the object of interest to obtain the Hscore of each molecule in each sample. Intergroup comparisons between the responding and nonresponding groups were performed by the Wilcoxon signed-rank test. There were three different expression patterns for immunihistochemical markers in enrolled 16 samples in our study. Firstly, high stainging rario and intensity of ADH1A in HCC tumor cells in the responders but not the nonresponders (Fig. 4A, P = 0.13). Secondly, there is a marker with insignificant difference of expression levels in the two groups, CD163 (Fig. 4C, P = 0.62). And thirdly, relatively high expression level of STING (Fig. 4B, P = 0.11), human leukocyte antigen-DRB (HLA_DRB, on both lymphocytes and tumor cells) (Fig. 4E, P = 0.22; Fig. 4F, P = 0.19) and CD8 (Fig. 4D, P = 0.15), were detected in the nonresponders, the first two molecules exhibit diffuse and strong positive signals.

HLA_DRB is a crucial component of MHC-II proteins [31,32], and its expression level represents, to some extent, the degree of immune activation [33]. In the mass spectrometry data, we also found that HLA_DRB1 showed an upregulation trend in the nonresponders (P = 0.1700, Fig. S4A). Unfortunately, the sample size was limited, and

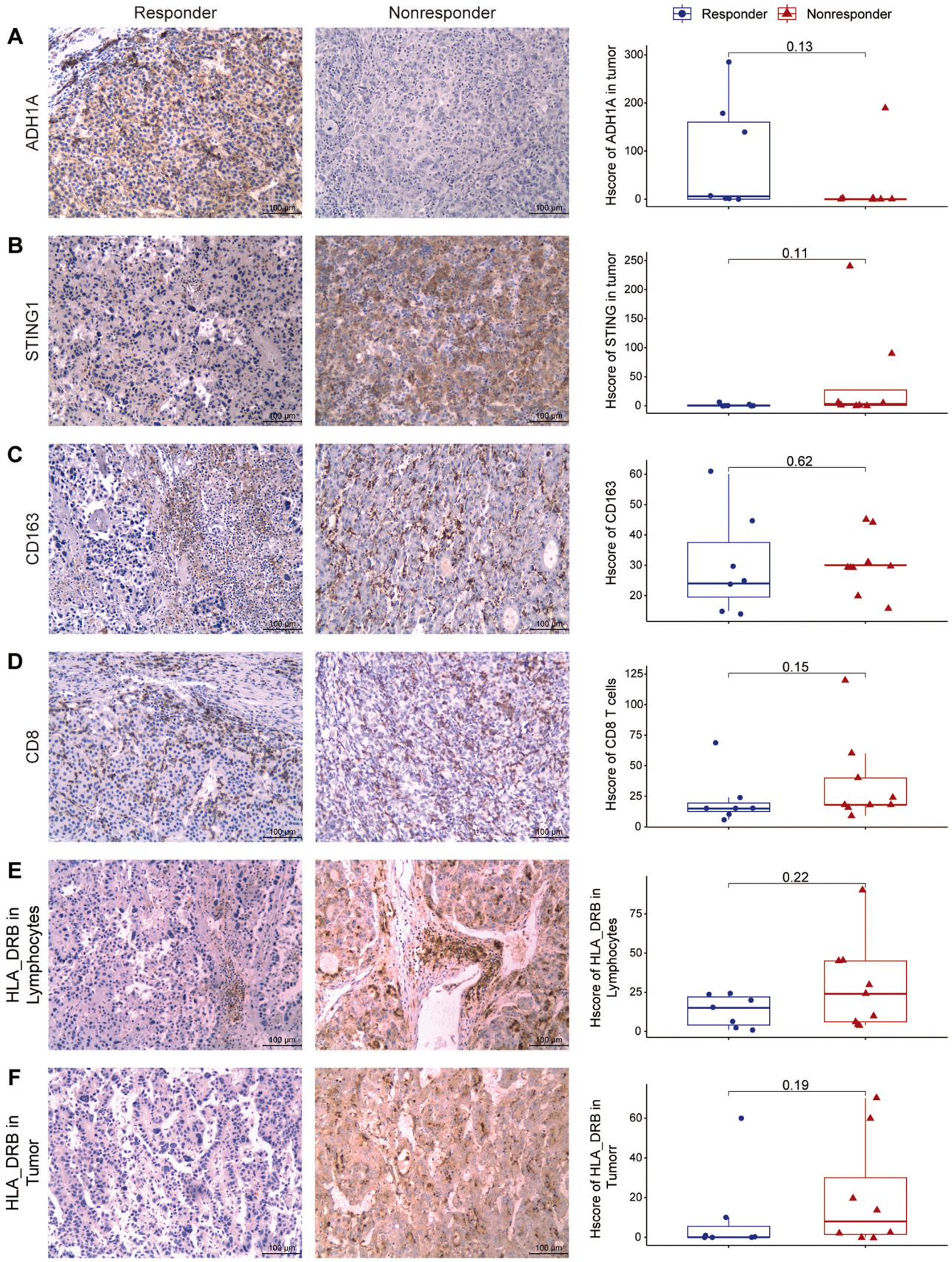

Fig. 4. IHC staining images and differences in the Hscore between the two groups. (A)-(F) Schematic representation of IHC staining results and the difference in the Hscore between the two groups, with positive staining shown by the tan color located in cell cytoplasm (ADH1A in the responding group, STING1), cell membrane and cytoplasm (CD163 and HLA_DRB), and cell membrane (CD8). The negative results of the above immunohistochemical detection were the only blue signals in cell nuclei stained by hematoxylin (eg. ADH1A in the nonresponding group).

the p-values for the intergroup comparisons of each molecule indicated that the differences were not significant. However, the trend was consistent with that found in the previous analysis. The Hscore for each molecule can be found in Table S11.

3.6. Molecules and pathways associated with sorafenib resistance correlate with the malignant features of HCC

We obtained the dataset for hepatitis B virus (HBV)- associated HCC published by Jia Fan et al. [25] and the dataset for early-stage HCC published by Fuchu He et al. [17] to increase the clinical applications values of molecules and pathways screened based on the sorafenib response/nonresponse status. In the HBV-associated HCC dataset, we transformed the proteomic expression profile data into pathway enrichment scores by ssGSEA and selected the pathways that were consistent with the specific differential pathways screened based on sorafenib response/nonresponse as the criteria for consensus clustering. Visually, the consensus matrix with a k value of 2 seemed to show the cleanest separation between clusters (Fig. S3A). The consensus cumulative distribution function (CDF) and delta area plots show that the area under the consensus CDF does not increase significantly as k increases from a value of 2 (Fig. S3B). The enrichment score of each pathway in each sample is shown on a heatmap. The tumor samples were generally classified as cluster 1, and the normal paracancer samples were generally classified as cluster 2. In addition, the pathways related to the drug nonresponse were enriched in the tumor samples and cluster 1, while the pathways related to the drug response were enriched in the normal samples and cluster 2 (Fig. 5A, Table S12). To determine cutoff values for survival analysis, clinical data from the early-stage HCC dataset were analyzed separately for STING1 protein expression and lysosome and cytosolic DNA sensing pathways, which represent autophagy, and for ADH1A protein expression and the pentose and glucuronate interconversions and ascorbate and aldarate metabolism pathways, which represent biotransformation (Fig. 5B-G). According to ADH1A (Fig. 5B, $P = 0.014$), pentose and glucuronate interconversions, ascorbate and aldarate metabolism and cytosolic DNA sensing pathways (Fig. 5D. Fig. 5D, $P = 0.039$; Fig. 5F, $P = 0.037$; Fig. 5G, $P = 0.0037$) showed significant differences in overall survival (OS) in patients with early-stage HCC between the high and low expression groups. After grouping according to the expression levels of STING1 (Fig. 5C, $P = 0.075$) and lysosome pathway (Fig. 5E, $P = 0.059$), the OS between the two groups also approached significant differences. High expression levels of the STING1 protein and activation levels of the lysosome and cytosolic DNA sensing pathways, which represent autophagy, were associated with poor prognosis. High expression levels of the ADH1A protein and activation levels of the pentose and glucuronate interconversions and ascorbate and aldarate metabolism pathways, which represent biotransformation, were associated with good prognosis.

4. Discussion and conclusions

As a first-line treatment for advanced HCC, sorafenib has a worse than expected patient benefit rate [34]. We explored how pretreatment protein expression patterns and activation of signaling pathways affect sorafenib resistance by proteomic characterization of pretreatment samples from sorafenib responders and nonresponders.

Among the differentially expressed proteins, we identified two key molecules, ADH1A and STING1. In the pathway enrichment analysis, autophagy-related pathways were enriched in the nonresponding group, while biotransformation-related pathways were enriched in the responding group. STING1, a core molecule mediating autophagy, is activated by the cell membrane DNA sensor cyclic GMP-AMP synthase (CGAS), and its acute activation facilitates antitumor therapeutic efficacy, while its chronic activation may mediate inflammation and promote tumor survival [27]. On the other hand, lysosomes are the central organelles of autophagy, meeting the energy needs of cells by degrading damaged organelles and long-lived proteins and attenuating cell death caused by endoplasmic reticulum (ER) stress [14].

The pathways enriched in the responding group are mainly related to the phase II reactions of biotransformation. Glucuronide in the pentose and glucuronate interconversions pathway plays an important role in conjugates detoxification of containing toxic substances [35]; L-ascorbic acid, in the ascorbate and aldarate metabolism pathway, is a potent antioxidant [36]. Both pathways were found to be significantly abnormal in a study of oxidative damage in the pancreas, suggesting that both pathways play a crucial role in resistance to oxidative stress [28,36]. Downregulation of specific biotransformation pathways can cause substrates to be shunted into the remaining pathways and result in damage. For example, ADH1A, a key enzyme in the metabolism of alcohol and retinol, is coupled to dehydrogenation of the cofactor NAD when it metabolizes its substrate and therefore does not produce oxygen radicals [37]. This observation explains the enrichment of nicotinate and nicotinamide metabolism in the responding group (Fig. 2B). When ADH1A is downregulated retinol becomes a substrate for P450s and generates oxygen radicals, as confirmed by a study that constructed an ADH1A-/- mouse model after feeding vitamin A found increased liver damage [37,38]; ethanol induces lipid peroxidation through the microsomal pathway, and its metabolic end products interfere with normal cellular metabolism, for example, Ciuclan L et al. found that lipid deposition, increased oxidative stress, and enhanced alcohol toxicity in cells treated with alcohol after knockdown of ADH1A in hepatocytes [39,40]. Therefore, the reduced biotransformation capacity increases hepatic oxidative damage to some extent, and oxidatively damaged DNA (e.g., 8-OHG-modified DNA) is a potent autophagy activator [29]. Therefore, we suggest that the reduced biotransformation capacity in the drug-nonresponding group partially promotes active autophagy in this group.

Pathway enrichment analysis also revealed activation of the redundant PI3K/AKT/mTOR pathway in the nonresponding group, with similar degrees of Ras/Raf/MAPK pathway activation in both groups. Therefore, we believe that in the nonresponding group, sorafenib's target in the pathway is successfully bypassed via promotion of angiogenesis through alternative pathways prior to treatment, a hypothesis consistent with the enrichment of VEGF signaling in the nonresponding group (Fig. 2B), may partially explain the abundance of endothelial and pericytes in the drug-nonresponding group observed by immuno-infiltration analysis. Thus, poor efficacy is to be expected. As previously described, mTOR represses ADH1A transcription by phosphorylating histone deacetylase 1 (HDAC1) (Fig. S4B) [30] and that mTOR inhibits autophagy [27]. Interestingly, it has been reported in cell line studies of both hepatocellular carcinoma and renal cell carcinoma that after inhibition of AKT and thus mTOR, autophagy was strongly activated and caused autophagy-dependent cell death (ADCD) in sorafenib-resistant cells [11,41]. Combining the results of redundant activation of the PI3K/AKT/mTOR pathway and downregulation of ADH1A in the nonresponding group and related mechanisms reported by other researchers, we propose a hypothetical model: a balance between STING1-mediated autophagy activation and PI3K/AKT/mTOR activation-induced autophagy inhibition is maintained in the nonresponding group to maintain the intensity of autophagic activity at a level that reduces ER stress and meets the energy requirements to promote tumor survival. Besides, activation of the redundant PI3K/AKT/mTOR pathway not only bypasses the target of sorafenib but also interferes with the decrease in the biotransformation capacity and the activation of autophagy in the nonresponding group. Collectively, the results of the immune infiltration analysis and immunohistochemical staining, indicated that

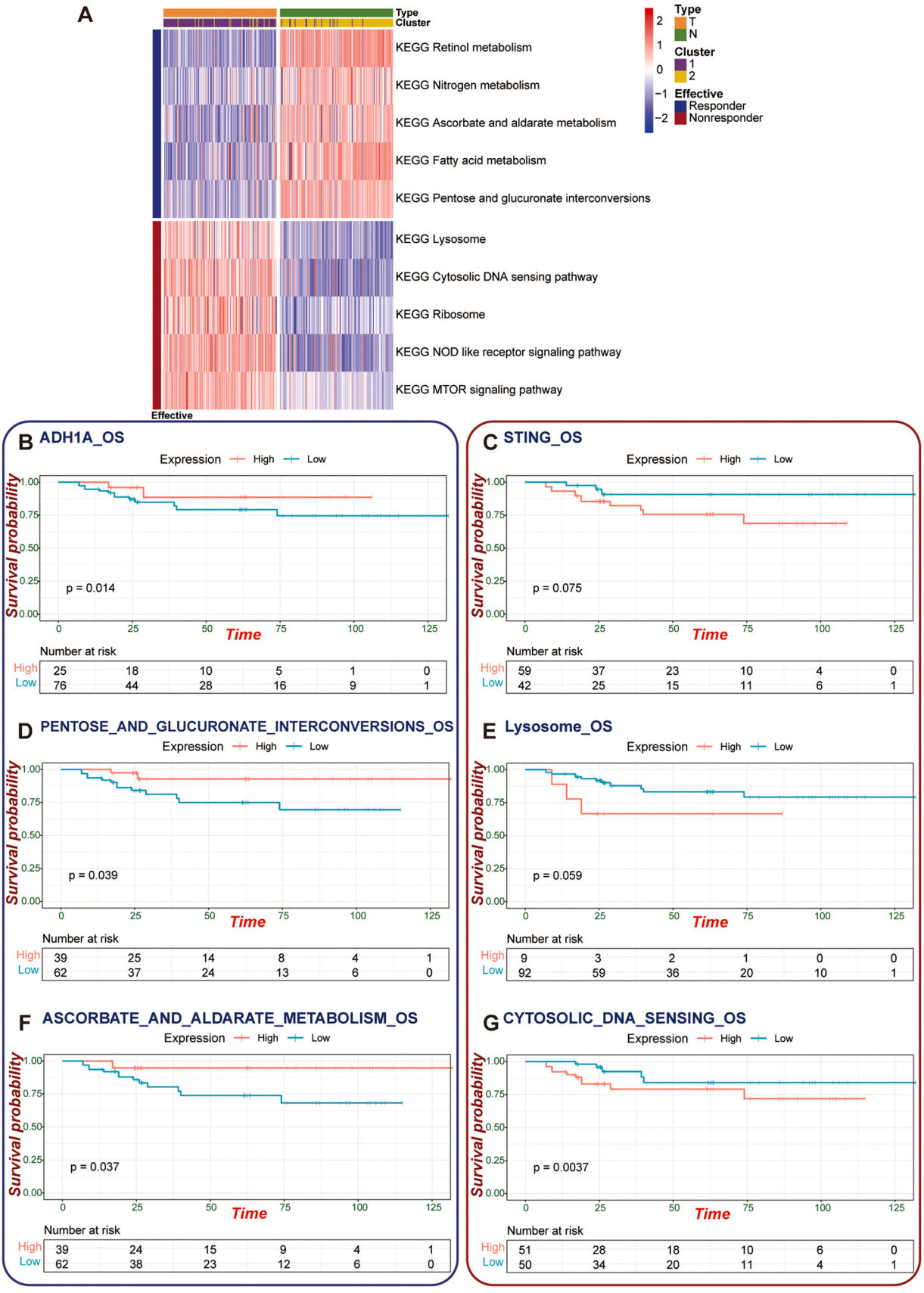

Fig. 5. Additional datasets were obtained for further validation. (A) Consensus clustering of data for HBV-associated HCC using differential pathways identified from our sorafenib data, the heatmap of the enrichment scores for each pathway in each sample, and annotation of clustering information, tissue origin, and corresponding pathways in the nonresponding/responding groups. (**B**)-(**G**) Survival analysis of differential molecules and pathways between the sorafenib nonresponding/responding groups in the data for early-stage HCC.

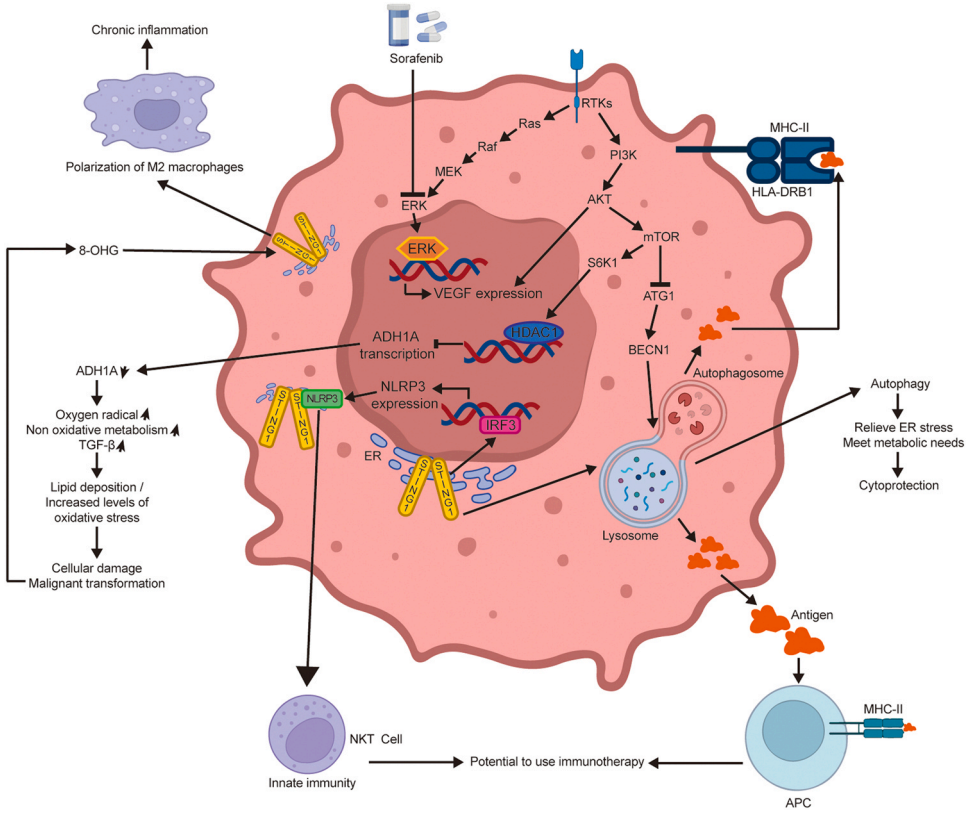

Fig. 6. Mechanisms by which some pretreatment factors influence sorafenib resistance.

innate immunocytes, immunosuppressive cells, and immunoreactive cells were abundant in the nonresponding group. Interestingly, the IHC staining intensity of CD163, a marker of M2 macrophages, was particularly nonsignificantly different between the two groups, suggesting that the difference in the abundance of infiltrating immunosuppressive M2 macrophages between the two groups may have been exaggerated in the immune infiltration analysis. STING signaling can regulate the NOD-like receptor signaling pathway through NOD-like receptor thermal protein domain associated protein 3 (NLRP3) to activate innate immunity [27,42]. Simultaneously, the resulting induction of chronic inflammation along with oxidative damage following the decrease in biotransformation capacity results in recruitment of tumor-associated macrophages (TAMs) [27,43]. However, in addition, the products of autophagy may contact antigen-presenting cells (APCs) as antigens or even be presented on the surface of tumor cells as endogenous proteins by MHC II molecules to activate adaptive immunity [32,44] as partially confirmed by immunohistochemical staining of HLA_DRB in lymphocytes and tumor cells (Fig. 4E-F). Combining the results of immune infiltration analysis and immunohistochemistry and the reported mechanisms related to autophagy affecting tumor immunity, we suggests that the benefit of immunotherapy in sorafenib-nonresponding patients with autophagy activation is worth exploring. Analysis of the extended dataset demonstrated that sorafenib response/nonresponse-related autophagy and biotransformation are also malignant features that distinguish HCC cells from normal hepatocytes and that the STING1 protein, the lysosome pathway, and the cytosolic DNA sensing pathway representing autophagy and the ADH1A protein, the pentose and glucuronate interconversions pathway, and the ascorbate and aldarate metabolism pathway representing biotransformation, have some prognostic value in HCC.

In summary, the degree of redundant PI3K/AKT/mTOR pathway activation, the biotransformation capacity, and the autophagy level in HCC patients prior to sorafenib treatment are likely to affect their sensitivity to sorafenib. These three aspects might interact mechanistically to promote tumor cell survival (Fig. 6). Patients with autophagy activation may benefit from immunotherapy in the setting of sorafenib resistance, while approaches that interfere with autophagic homeostasis, such as modulation of redundant pathways, may reverse resistance via multiple mechanisms, and enhancing biotransformation in HCC patients may contribute to prolonged survival. These molecules and pathways are also potential markers for predicting sorafenib efficacy.

Ethical approval

Ethical approval was obtained from the Ethics Committee of Cancer Hospital, Chinese Academy of Medical Sciences (#20/455–2651).

Funding

This work was supported by the National Key Research and Development Program of China (2022YFE0103600) and Research funding from Cancer Hospital, Chinese Academy of Medical Sciences (LC2020A12).

CRediT authorship contribution statement

Ruiqi Zheng: Conceptualization, Software, Formal analysis, Investigation, Data curation, Writing – original draft, Writing – review & editing. **Shuang Weng:** Software, Formal analysis, Writing – original draft, Writing – review & editing. **Jianping Xu:** Methodology, Writing – review & editing. **Zhuo Li:** Writing – review & editing. **Yaru Wang:** Writing – review & editing. **Zulihumaer Aizimuaji:** Writing – review & editing. **Sheng Ma:** Writing – review & editing. **Linlin Zheng:** Writing – review & editing. **Haiyang Li:** Writing – review & editing. **Wantao Ying:** Resources, Writing –

review & editing. **Weiqi Rong:** Resources, Writing – review & editing. **Ting Xiao:** Conceptualization, Resources, Writing – review & editing, Supervision, Project administration, Funding acquisition. All authors have read and approved the final manuscript.

Data availability

The MS proteomics data generated in this study have been deposited in the ProteomeXchange Consortium (http://proteomecentral.proteomexchange.org) via the iProX partner repository (http://iprox.cn) with the dataset identifiers PXD040371 and IPX0005954000.

Declaration of Competing Interest

The authors declare no competing interests.

Acknowledgements

The authors acknowledge Dr. Huiqin Guo and Dr. Huan Zhao for their professional pathological opinions, as well as the study investigators for their contributions to this study.

Appendix A. Supporting information

Supplementary data associated with this article can be found in the online version at doi:10.1016/j.csbj.2023.07.005.

References

[1] Sung H, Ferlay J, Siegel RL, Laversanne M, Soerjomataram I, et al. Global Cancer Statistics 2020: GLOBOCAN estimates of incidence and mortality worldwide for 36 cancers in 185 countries. CA Cancer J Clin 2021;71:209–49.
[2] Cheng Z, Wei-Qi J, Jin D. New insights on sorafenib resistance in liver cancer with correlation of individualized therapy. Biochim Biophys Acta Rev Cancer 2020;1874:188382.
[3] Tang W, Chen Z, Zhang W, Cheng Y, Zhang B, et al. The mechanisms of sorafenib resistance in hepatocellular carcinoma: theoretical basis and therapeutic aspects. Signal Transduct Target Ther 2020;5:87.
[4] Abdelgalil AA, Alkahtani HM, Al-Jenoobi FI Sorafenib. Profiles Drug Subst Excip Relat Method 2019;44:239–66.
[5] He Y, Luo Y, Huang L, Zhang D, Wang X, et al. New frontiers against sorafenib resistance in renal cell carcinoma: from molecular mechanisms to predictive biomarkers. Pharm Res 2021;170:105732.
[6] Wilhelm SM, Carter C, Tang L, Wilkie D, McNabola A, et al. BAY 43-9006 exhibits broad spectrum oral antitumor activity and targets the RAF/MEK/ERK pathway and receptor tyrosine kinases involved in tumor progression and angiogenesis. Cancer Res 2004;64:7099–109.
[7] Psyrri A, Arkadopoulos N, Vassilakopoulou M, Smyrniotis V, Dimitriadis G. Pathways and targets in hepatocellular carcinoma. Expert Rev Anticancer Ther 2012;12:1347–57.
[8] Liu J, Qiu WC, Shen XY, Sun GC. Bioinformatics analysis revealed hub genes and pathways involved in sorafenib resistance in hepatocellular carcinoma. Math Biosci Eng 2019;16:6319–34.
[9] Tang TC, Man S, Xu P, Francia G, Hashimoto K, et al. Development of a resistance-like phenotype to sorafenib by human hepatocellular carcinoma cells is reversible and can be delayed by metronomic UFT chemotherapy. Neoplasia 2010;12:928–40.
[10] Sun H, Wang F, Huang Y, Wang J, Zhang L, et al. Targeted inhibition of ACLY expression to reverse the resistance of sorafenib in hepatocellular carcinoma. J Cancer 2022;13:951–64.
[11] Liu S, Gao M, Wang X, Ding S, Lv J, et al. Ubenimex attenuates acquired sorafenib resistance in renal cell carcinoma by inhibiting Akt signaling in a lipophagy associated mechanism. Oncotarget 2016;7:79141–53.
[12] Sheng Y, Ng CP, Lourie R, Shah ET, He Y, et al. MUC13 overexpression in renal cell carcinoma plays a central role in tumor progression and drug resistance. Int J Cancer 2017;140:2351–63.
[13] Cai S, Fu S, Zhang W, Yuan X, Cheng Y, et al. SIRT6 silencing overcomes resistance to sorafenib by promoting ferroptosis in gastric cancer. Biochem Biophys Res Commun 2021;577:158–64.
[14] Liu J, Fan L, Wang H, Sun G. Autophagy, a double-edged sword in anti-angiogenesis therapy. Med Oncol 2016;33:10.
[15] Omiecinski CJ, Vanden Heuvel JP, Perdew GH, Peters JM. Xenobiotic metabolism, disposition, and regulation by receptors: from biochemical phenomenon to predictors of major toxicities. Toxicol Sci 2011;120(Suppl 1):S49–75.
[16] Wiśniewski JR, Zougman A, Nagaraj N, Mann M. Universal sample preparation method for proteome analysis. Nat Methods 2009;6:359–62.
[17] Jiang Y, Sun A, Zhao Y, Ying W, Sun H, et al. Proteomics identifies new therapeutic targets of early-stage hepatocellular carcinoma. Nature 2019;567:257–61.
[18] Weng S, Wang M, Zhao Y, Ying W, Qian X. Optimised data-independent acquisition strategy recaptures the classification of early-stage hepatocellular carcinoma based on data-dependent acquisition. J Proteom 2021;238:104152.
[19] van Buuren S, Groothuis-Oudshoorn K. Mice: multivariate imputation by chained equations in R. J Stat Softw 2011;45:1–67.
[20] Ritchie ME, Phipson B, Wu D, Hu Y, Law CW, et al. limma powers differential expression analyses for RNA-sequencing and microarray studies. Nucleic Acids Res 2015;43:e47.
[21] Yu G, Wang L-G, Han Y, He Q-Y. clusterProfiler: an R package for comparing biological themes among gene clusters. OMICS 2012;16:284–7.
[22] Hänzelmann S, Castelo R, Guinney J. GSVA: gene set variation analysis for microarray and RNA-seq data. BMC Bioinforma 2013;14:7.
[23] Aran D, Hu Z, Butte AJ. xCell: digitally portraying the tissue cellular heterogeneity landscape. Genome Biol 2017;18:220.
[24] Wilkerson MD, Hayes DN. ConsensusClusterPlus: a class discovery tool with confidence assessments and item tracking. Bioinformatics 2010;26:1572–3.
[25] Gao Q, Zhu H, Dong L, Shi W, Chen R, et al. Integrated proteogenomic characterization of HBV-Related hepatocellular carcinoma. Cell 2019:179.
[26] Gui X, Yang H, Li T, Tan X, Shi P, et al. Autophagy induction via STING trafficking is a primordial function of the cGAS pathway. Nature 2019;567:262–6.
[27] Zhang R, Kang R, Tang D. The STING1 network regulates autophagy and cell death. Signal Transduct Target Ther 2021;6:208.
[28] Salau VF, Erukainure OL, Koorbanally NA, Islam MS. Kolaviron modulates dysregulated metabolism in oxidative pancreatic injury and inhibits intestinal glucose absorption with concomitant stimulation of muscle glucose uptake. Arch Physiol Biochem 2020.
[29] Hopfner K-P, Hornung V. Molecular mechanisms and cellular functions of cGAS-STING signalling. Nat Rev Mol Cell Biol 2020;21:501–21.
[30] Zahid KR, Yao S, Khan ARR, Raza U, Gou D. mTOR/HDAC1 crosstalk mediated suppression of ADH1A and ALDH2 links alcohol metabolism to hepatocellular carcinoma onset and progression. Front Oncol 2019;9:1000.
[31] Stern LJ, Brown JH, Jardetzky TS, Gorga JC, Urban RG, et al. Crystal structure of the human class II MHC protein HLA-DR1 complexed with an influenza virus peptide. Nature 1994;368:215–21.
[32] Axelrod ML, Cook RS, Johnson DB, Balko JM. Biological consequences of MHC-II expression by tumor cells in cancer. Clin Cancer Res 2019;25:2392–402.
[33] Kitamura H, Ohno Y, Toyoshima Y, Ohtake J, Homma S, et al. Interleukin-6/STAT3 signaling as a promising target to improve the efficacy of cancer immunotherapy. Cancer Sci 2017;108:1947–52.
[34] Sui Z-g, Xue H-w, Jing F-b, Leng P. Sorafenib plus capecitabine for patients with advanced hepatocellular caicinoma. China Pharm 2008:848–9.
[35] Sun H, Zhang A-H, Song Q, Fang H, Liu X-Y, et al. Functional metabolomics discover pentose and glucuronate interconversion pathways as promising targets for Yang Huang syndrome treatment with Yinchenhao Tang. RSC Adv 2018;8:36831–9.
[36] Shi K, Zhao Q, Shao M, Duan Y, Li D, et al. Untargeted metabolomics reveals the effect of selective breeding on the quality of chicken meat. Metabolites 2022:12.
[37] Molotkov A, Fan X, Duester G. Excessive vitamin a toxicity in mice genetically deficient in either alcohol dehydrogenase Adh1 or Adh3. Eur J Biochem 2002;269:2607–12.
[38] Molotkov A, Deltour L, Foglio MH, Cuenca AE, Duester G. Distinct retinoid metabolic functions for alcohol dehydrogenase genes Adh1 and Adh4 in protection against vitamin A toxicity or deficiency revealed in double null mutant mice. J Biol Chem 2002;277:13804–11.
[39] Ciuclan L, Ehnert S, Ilkavets I, Weng H-L, Gaitantzi H, et al. TGF-beta enhances alcohol dependent hepatocyte damage via down-regulation of alcohol dehydrogenase I. J Hepatol 2010;52:407–16.
[40] Wu H, Cai P, Clemens DL, Jerrells TR, Ansari GAS, et al. Metabolic basis of ethanol-induced cytotoxicity in recombinant HepG2 cells: role of nonoxidative metabolism. Toxicol Appl Pharmacol 2006;216:238–47.
[41] Zhai B, Hu F, Jiang X, Xu J, Zhao D, et al. Inhibition of Akt reverses the acquired resistance to sorafenib by switching protective autophagy to autophagic cell death in hepatocellular carcinoma. Mol Cancer Ther 2014;13:1589–98.
[42] Liu D, Wu H, Wang C, Li Y, Tian H, et al. STING directly activates autophagy to tune the innate immune response. Cell Death Differ 2019;26:1735–49.
[43] Dai E, Han L, Liu J, Xie Y, Zeh HJ, et al. Ferroptotic damage promotes pancreatic tumorigenesis through a TMEM173/STING-dependent DNA sensor pathway. Nat Commun 2020;11:6339.
[44] Abelin JG, Harjanto D, Malloy M, Suri P, Colson T, et al. Defining HLA-II ligand processing and binding rules with mass spectrometry enhances cancer epitope prediction. Immunity 2019:51.